STRUCTURAL BIOLOGY

D_4 dopamine receptor high-resolution structures enable the discovery of selective agonists

Sheng Wang,[1]*† Daniel Wacker,[1]*† Anat Levit,[2]* Tao Che,[1] Robin M. Betz,[3,4,5,6] John D. McCorvy,[1] A. J. Venkatakrishnan,[3,4,5] Xi-Ping Huang,[1] Ron O. Dror,[3,4,5,6] Brian K. Shoichet,[2]† Bryan L. Roth[1,7,8]†

Dopamine receptors are implicated in the pathogenesis and treatment of nearly every neuropsychiatric disorder. Although thousands of drugs interact with these receptors, our molecular understanding of dopaminergic drug selectivity and design remains clouded. To illuminate dopamine receptor structure, function, and ligand recognition, we determined crystal structures of the D_4 dopamine receptor in its inactive state bound to the antipsychotic drug nemonapride, with resolutions up to 1.95 angstroms. These structures suggest a mechanism for the control of constitutive signaling, and their unusually high resolution enabled a structure-based campaign for new agonists of the D_4 dopamine receptor. The ability to efficiently exploit structure for specific probe discovery—rapidly moving from elucidating receptor structure to discovering previously unrecognized, selective agonists—testifies to the power of structure-based approaches.

Dopamine (DA) receptors are G protein–coupled receptors (GPCRs) that are therapeutic targets for treating schizophrenia, Parkinson's disease, and drug abuse (*1*). DA receptors are divided into two subfamilies: the $G\alpha_{s/olf}$-coupled D_1-like family (e.g., D_1 and D_5 dopamine receptors) and the $G\alpha_{i/o}$-coupled D_2-like family [e.g., D_2, D_3, and D_4 dopamine receptors (DRD2, DRD3, and DRD4)] (*2*). Given that DRD4 has been implicated in many disorders, including attention deficit disorder, metastatic progression, and erectile dysfunction, DRD4-selective drugs have therapeutic promise (*2*). Although >10,000 molecules are reported to have DA receptor activity (data S1), our understanding of the molecular mechanisms for DA receptor selectivity and activity is incomplete, because only a relatively low-resolution structure of DRD3 has been reported (*3*).

To obtain well-ordered crystals for high-resolution studies of human DRD4 in complex with nemonapride, we replaced residues 228 to 336 of ICL3 (intracellular loop 3) with thermostabilized BRIL (apocytochrome b562RIL) (*4*), yielding DRD4-BRIL, which has a binding affinity for ^{3}H-*N*-methylspiperone similar to that of native DRD4 (table S1). The DRD4-nemonapride complex crystals diffracted to 1.95-Å resolution (figs. S1 and S2 and table S2), revealing a large network of water molecules and ions (Fig. 1A). The most dramatic structural differences between DRD3 (Protein Data Bank ID, 3PBL) and DRD4 are in ECL3 (extracellular loop 3), the extracellular ends of TMs (transmembrane helices) VI and VII, and the intracellular ends of TMs III and V (fig. S3). Compared with DRD3, in DRD4, TMs VI and VII are further apart, and the extracellular tip of TM VI is located ~2 Å closer to TM V (fig. S3). The position of DRD3's TM VI appears fixed by an interhelical hydrogen bond between $Y365^{7.35}$ and $H349^{6.55}$, whereas in DRD4, $V430^{7.35}$ cannot hydrogen-bond with $H414^{6.55}$ (fig. S3). Given the critical nature of TMs V and VI in GPCR activation (*5*), we wondered whether this added hydrogen-bond restraint has functional consequences. A $V430^{7.35}$Y mutation in DRD4, recapitulating DRD3's interhelical hydrogen bond, increased DRD4 constitutive activity (fig. S4A), whereas the $Y365^{7.35}$V mutation in DRD3, mimicking the DRD4 configuration, reduced DRD3 constitutive activity (fig. S4B). Meanwhile, $H^{6.55}$ occupies different rotamer states in DRD4 and DRD3, which could lead to differential ligand binding and activity between the two subtypes, because $H^{6.55}$ forms a direct hydrogen bond with eticlopride in DRD3 (*3*) and water-mediated contacts with nemonapride in DRD4 (Fig. 1, B and C).

High-resolution structures of the A_{2A} adenosine (A_{2A}AR) (Fig. 2A) (*6*), δ-opioid (δ-OR) (Fig. 2A) (*7*), β_1-adrenergic (β_1AR) (*8*), and protease-activated (PAR1) (*9*) receptors revealed a conserved Na^+-water cluster, coordinated by two highly conserved residues, $D^{2.50}$ and $S^{3.39}$ (*10*). We determined structures of the DRD4-nemonapride complex with or without ~200 mM added sodium and observed an electron density for sodium only when it was added during crystallization (Fig. 2A and fig. S5). This provides direct structural evidence for the presence of a sodium ion in its binding site [discussed in (*10*)]. Importantly, the DRD4 construct used for crystallization displayed similar sodium-dependent allosteric regulation to the wild type (fig. S6A). Similar to A_{2A}AR and δ-OR, sodium formed a salt bridge with $D80^{2.50}$ and made polar interactions with $S122^{3.39}$ and two water molecules in DRD4 (Fig. 2A). A previously described third coordinating water was not observed, likely owing to the lower resolution of 2.15 Å (Fig. 2A); the β_1AR 2.1-Å structure also showed weaker density for this water molecule relative to those in the structures of δ-OR and A_{2A}AR (*8*). Compared with other tested GPCRs, DRD4 had lower sodium affinity than δ-OR, μ-OR, or A_{2A}AR (Fig. 2, B to E, and fig. S6). As expected (*7*), lowering [Na^+] potentiated DRD4 constitutive activity in a nemonapride-sensitive fashion (fig. S7).

The sodium pocket in DRD4 adopts nearly identical conformations in the sodium-bound and sodium-free states (root mean square deviation of 0.084 Å, calculated over $D80^{2.50}$, $L118^{3.35}$, $S122^{3.39}$, and four water molecules) (Fig. 2A). Correspondingly, molecular dynamics (MD) simulations of the inactive state showed that the sodium-free pocket does not collapse even when nemonapride is absent (fig. S8). Instead, the pocket fills with water, and $D80^{2.50}$ and $S122^{3.39}$ become more mobile, although their average positions remain similar to those observed with sodium bound (fig. S8). MD simulations also predicted that sodium's position and mobility would be affected by nemonapride (fig. S9A). With nemonapride bound, sodium mostly occupies a cluster of positions surrounding its crystallographic pose, but it occasionally binds a second cluster about 2.5 Å closer to nemonapride, as observed in other GPCRs (*11*, *12*). In simulations of nemonapride-free DRD4, sodium transitioned more frequently between clusters and spent more time in the second cluster, occasionally even occupying the now-empty ligand-binding site (figs. S9A, S10, and S11). In both clusters, coordination to $D80^{2.50}$ and $S122^{3.39}$ was largely maintained, with the side-chain hydroxyl of $S122^{3.39}$ rotating toward sodium. Simulations also indicated that nemonapride's binding pose is more stable in the presence of sodium (fig. S9B), in agreement with the higher affinity of nemonapride-like ligands in the presence of sodium (*13*, *14*).

Nemonapride interacts with the conserved aspartate $D115^{3.32}$, and its benzamide ring binds within a conserved orthosteric binding pocket (OBP) lined by residues from TMs II, III, V, VI, and VII and ECL2 (Fig. 1, B and C). Nemonapride's conformation is constrained by an intramolecular hydrogen bond between its amide nitrogen and the methoxy substituent of the benzyl ring. Nemonapride's methoxy ring is fixed by intermolecular contacts with side chains of the conserved residues $F411^{6.52}$ and $V116^{3.33}$ and by a hydrogen bond with the side chain of $S196^{5.42}$

[1]Department of Pharmacology, University of North Carolina at Chapel Hill, Chapel Hill, NC 27599-7365, USA. [2]Department of Pharmaceutical Chemistry, University of California, San Francisco, San Francisco, CA 94158-2280, USA. [3]Department of Computer Science, Stanford University, CA 94305, USA. [4]Department of Molecular and Cellular Physiology, Stanford University School of Medicine, Stanford, CA 94305, USA. [5]Institute for Computational and Mathematical Engineering, Stanford University, Stanford, CA 94305, USA. [6]Biophysics Program, Stanford University, Stanford, CA 94305, USA. [7]Division of Chemical Biology and Medicinal Chemistry, Eshelman School of Pharmacy, University of North Carolina at Chapel Hill, Chapel Hill, NC 27599-7360, USA. [8]National Institute of Mental Health Psychoactive Drug Screening Program, School of Medicine, University of North Carolina at Chapel Hill, Chapel Hill, NC 27599-7365, USA.
*These authors contributed equally to this work. **†Corresponding author. Email: shengunc@email.unc.edu (S.W.); dwacker@email.unc.edu (D.W.); bshoichet@gmail.com (B.K.S.); bryan_roth@med.unc.edu (B.L.R.)**

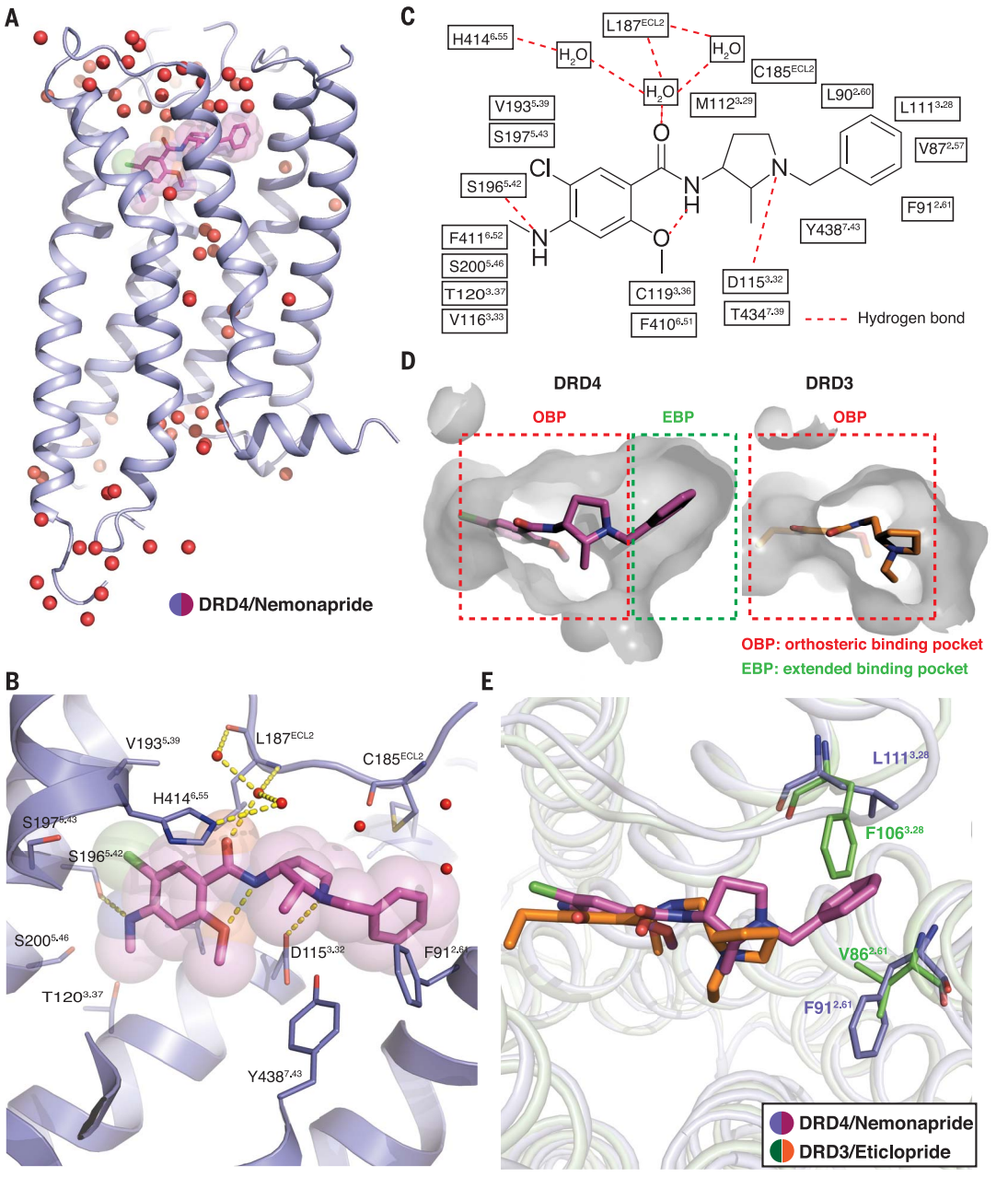

Fig. 1. Human DRD4-nemonapride complex crystal structure. (**A**) Overview of the DRD4-nemonapride complex structure, with water molecules depicted as red spheres. (**B**) Conformation of the binding pocket, with nemonapride shown as sticks with magenta carbons. The protein is displayed in cartoon representation, with the 11 contact residues within 4.0 Å from the ligand shown as slate-blue sticks. Structured water molecules are shown as red spheres. Ballesteros-Weinstein numbering is shown in superscript. (**C**) Diagram of ligand interactions in the binding pocket side chains at a 4.0-Å cutoff. Hydrogen bonds are shown with dashed lines. (**D**) Side views of the sliced binding pocket in the DRD4-nemonapride and DRD3-eticlopride complexes. The pocket surfaces are colored gray. Ligands are shown as capped sticks with carbons colored magenta (nemonapride) and orange (eticlopride). (**E**) Structural differences in the EBPs of DRD4 (slate blue) and DRD3 (green). Ligands are colored as in (D). Single-letter abbreviations for the amino acid residues are as follows: A, Ala; C, Cys; D, Asp; E, Glu; F, Phe; G, Gly; H, His; I, Ile; K, Lys; L, Leu; M, Met; N, Asn; P, Pro; Q, Gln; R, Arg; S, Ser; T, Thr; V, Val; W, Trp; and Y, Tyr.

(Fig. 1C). Nemonapride's unsubstituted benzyl group interacts with nonconserved residues $V87^{2.57}$, $L90^{2.60}$, $F91^{2.61}$, and $L111^{3.28}$, all of which have been implicated by mutagenesis for specifying DRD4 pharmacology (*15*, *16*). In the DRD4 structure, these residues emerge as part of a previously uncharacterized extended binding pocket (EBP) bordered by residues of TMs II and III (Fig. 1, B and C), distinct from that reported for DRD3 (*3*, *17*, *18*) (Fig. 1D). This DRD4 EBP is poorly conserved among the closely related members of the D_2-like subfamily (fig. S12) and reaches deep into the OBP-adjacent position between TMs II and III (Fig. 1, D and E). The DRD4 and DRD3 EBPs are thus distinct in shape and size (Fig. 1D). At the core of both is a crevice formed by residues 2.61 and 3.28. In DRD4, nemonapride's unsubstituted benzyl group is wedged between $F91^{2.61}$ and $L111^{3.28}$, indicating that its binding to DRD3 likely requires structural rearrangements to avoid clashes with $V86^{2.61}$ and $F106^{3.28}$ (Fig. 1E).

Docking DRD4-selective ligands against the DRD4 structure revealed that their aryl rings dock into the EBP, connecting directly and rigidly to the aminergic heterocycles of the antagonists, unlike nemonapride, which is nonselective. Because docking forces these rings into contact with specificity residues 2.61 and 3.28 (fig. S13), we hypothesized that steric clashes with $F^{3.28}$, and lack of interactions with $V^{2.61}$ in DRD3 and DRD2, contribute to DRD4 selectivity. Introducing a $F^{2.61}V/L^{3.28}F$ double substitution in DRD4 to mimic the DRD2 and DRD3 configuration attenuated affinities of DRD4-selective compounds, with nonselective compounds relatively unaffected (tables S1, S3, and S4). Introduction of the reverse double mutant into DRD2 ($V^{2.61}F/F^{3.28}L$) increased the affinity for DRD4-selective ligands without altering the affinities of nonselective compounds (tables S5 to S7), providing an atomic-resolution model of DRD4 ligand selectivity (Fig. 1E and fig. S13).

The structural definition of the EBP afforded us the opportunity to seek previously unrecognized DRD4-selective agonists with functional properties distinct from those of existing compounds, including biased agonists. Accordingly, we docked a library of more than 600,000 cationic, "lead-like" (*19*) molecules from ZINC (http://zinc15.docking.org) (*20*) against the 1.95-Å DRD4 structure. We sought

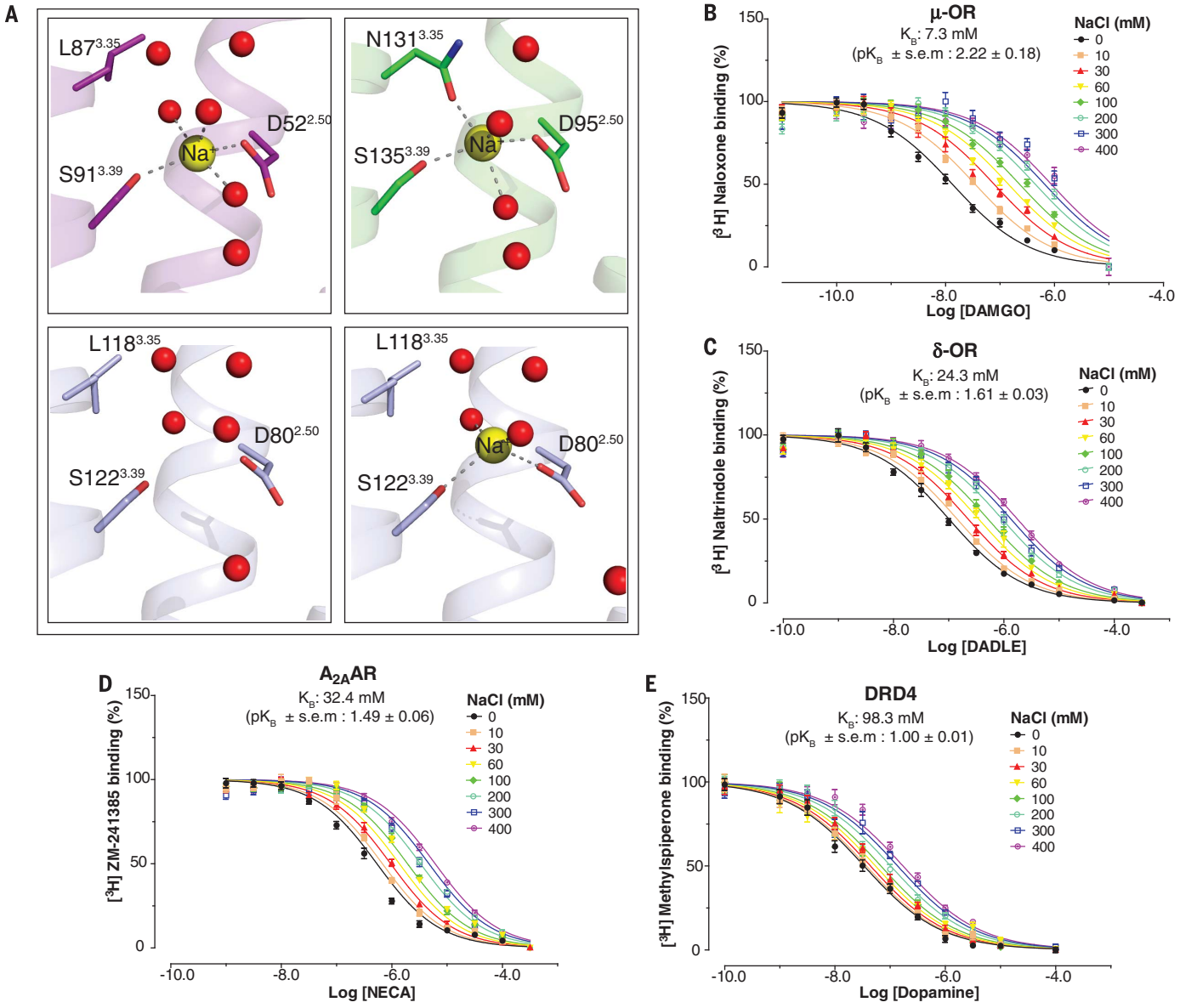

Fig. 2. Structural and functional details of the DRD4's allosteric Na^+ site. (**A**) Close-ups of respective Na^+ allosteric pockets in $A_{2A}AR$ (magenta), δ-OR (green), sodium-free DRD4 (slate blue, left), and sodium-bound DRD4 (slate blue, right). Receptors are shown as transparent cartoons, and residues lining the Na^+ cavity are shown as sticks and labeled according to the Ballesteros-Weinstein scheme. Water molecules in the cluster are shown as red spheres. Na^+ is displayed as a yellow sphere. The salt bridge between Na^+ and $D^{2.50}$ and hydrogen bonds are shown as gray dotted lines. (**B** to **E**) The allosteric effect of graded concentrations of sodium on DAMGO, DADLE, NECA, or dopamine affinity were respectively measured at μ-OR (B), δ-OR (C), $A_{2A}AR$ (D), and DRD4 (E). K_B, equilibrium dissociation constant of modulator binding to its allosteric site. Error bars, SEM.

(i) molecules that bound in both the OBP and EBP, reasoning that interactions with DRD4's EBP might confer selectivity (Fig. 3A and methods), and (ii) molecules that were unrelated to previously known ligands, reasoning that chemotypes that have not been studied in this context might exhibit previously unobserved biology (*21*, *22*). Of the 10 highest-ranking molecules tested (Fig. 3B and table S8), ***3*** and **9** were submicromolar agonists, with **9** being DRD4-selective (table S9). Both ***3*** and **9** are topologically dissimilar to dopaminergic ligands cataloged in ChEMBL20 (*23*), with the molecule most related to **9** having a Tanimoto coefficient of 0.27, suggesting that they represent different families (*22*) (table S9). Although ***3*** and **9** are dissimilar from one another, they share a motif in which the central aminergic nitrogen is separated by two carbons from a hydrogen-donating amine, which makes a bifurcated hydrogen bond to $D115^{3.32}$ (Fig. 3, C and D). The observation that agonists emerged from a screen against an inactive receptor state is unexpected, although not unprecedented (*21*, *24*). This may reflect the small conformational changes within the orthosteric site between active and inactive states (*21*), allowing for a broader recognition of molecules, at least in docking screens. As important may be the insistence on previously untested chemical entities, which favors diverse functional properties in the newly recognized ligands.

To optimize **9,** 75 analogs from ZINC were docked, and 15 were prioritized for testing on the basis of docking score, EBP occupancy, interaction with predicted arrestin-biasing residue $L187^{ECL2}$ (*25*), and diversity (table S10). All retained the quinolone and aminergic moieties, which engage key residues of the OBP, with most variations in the side chain predicted to interact with EBP residues. For example, compounds **9-6** and **9-11** (Fig. 4A and table S9) retained the quinolone heterocycle and the bidentate amino groups, with the hydroxymethyl replaced by simple extended side chains. While retaining major interactions of the quinolone heterocycle with the OBP, the increased flexibility of these analogs

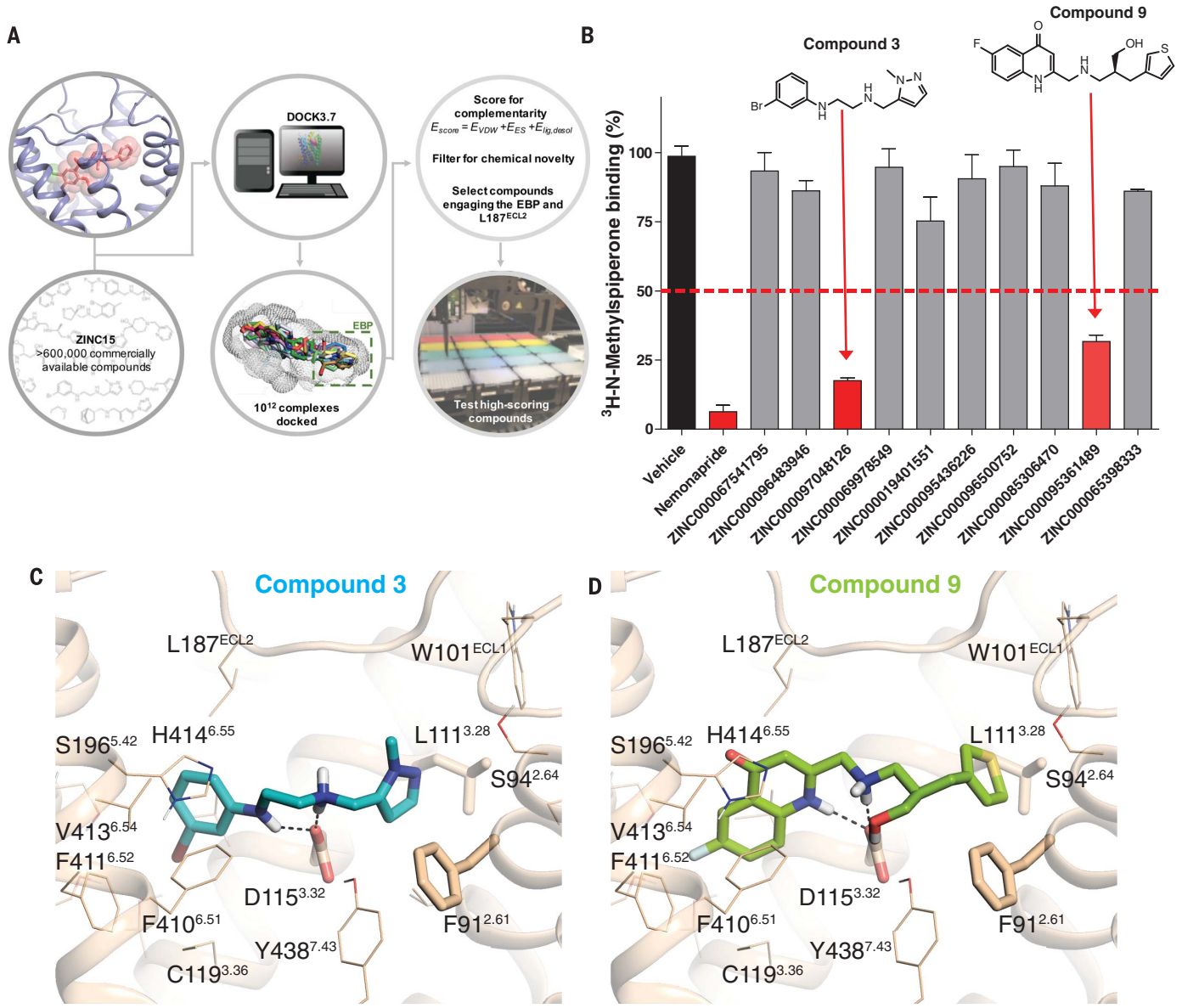

Fig. 3. Structure-guided discovery of selective DRD4 agonists. (**A**) Structure-based strategy for discovery of DRD4 chemotypes from docking screens of large virtual libraries (E_{ES}, electrostatic energy; E_{VDW}, van der Waals interaction energy; $E_{lig,desol}$, ligand desolvation energy). (**B**) Single-point competition binding assay of 10 candidate molecules against the DRD4 antagonist ^{3}H-*N*-methylspiperone. Each ligand was tested at 5 μM, and the data shown are means ± SEM (n = 3 measurements). (**C** and **D**) Docking poses of compounds **3** (C) and **9** (D). DRD4 is shown in tan, and compounds are shown as capped sticks with carbons colored cyan (compound **3**) and green (compound **9**). Ballesteros-Weinstein numbering is shown in superscript.

facilitated better packing against the specificity-determining EBP of DRD4 (Fig. 4B and fig. S14A). **9-6** and **9-11** had inhibition constants (K_i) that were improved 20-fold relative to that of **9** and lost detectable binding at DRD2 or DRD3 at 10 μM (Fig. 4, A and B; fig. S14A; and table S9). They are potent DRD4 partial agonists with arrestin-bias factors of 20- and 7.8-fold versus quinpirole (Fig. 4D and fig. S14B). This bias is consistent with the docking, which selected for interactions with L187^{ECL2} (*25*) and with which the conserved quinolone interacts (Fig. 4B and fig. S14A). EBP residue mutations disrupted the affinities of the newly discovered agonists (table S9), consistent with their docked poses (Fig. 4B and fig. S14A).

To further this series and increase compound affinity and selectivity, we docked 169 analogs of **9-6** and **9-11**, with a particular focus on chemically diverse moieties predicted to interact with the EBP. Of 27 docked compounds assayed, the most potent compound, **9-6-24**, exhibited a K_i of 3 nM, with no measurable affinity for DRD2, DRD3, or the EBP DRD4 mutant F$^{2.61}$V/L$^{3.28}$F, resulting in an increased selectivity of >3300-fold (tables S9 and S11). **9-6-24** has a phenolic ether oxygen (Fig. 4A), which appears to form an internal hydrogen bond with the amine, thus positioning the distal aryl ring over the non-conserved F91$^{2.61}$ in the EBP (Fig. 4C). With respect to quinpirole, **9-6-24** is a partial agonist with a 7.4-fold bias toward arrestin over G$\alpha_{i/o}$ signaling (Fig. 4E and fig. S15), which contrasts with most existing DRD4 agonists that are either balanced or slightly G protein–biased (fig. S16). Given that neither the parent compound **9-6** nor **9-6-24** displayed agonist activity at 320 nonolfactory GPCRs at 1 μM (Fig. 4, F and G), **9-6-24** is among the most potent and specific DRD4 agonists characterized.

Unlike its selectivity, the agonism or bias of **9-6-24** was not initially purposely designed (although we did focus on putatively biasing the contact residue), but rather was a result of our focus on untested chemical entities followed by experimental selection of these desired features. We are making **9-6-24** and a negative control molecule with 1/2500th the affinity (**9-6-16**) openly

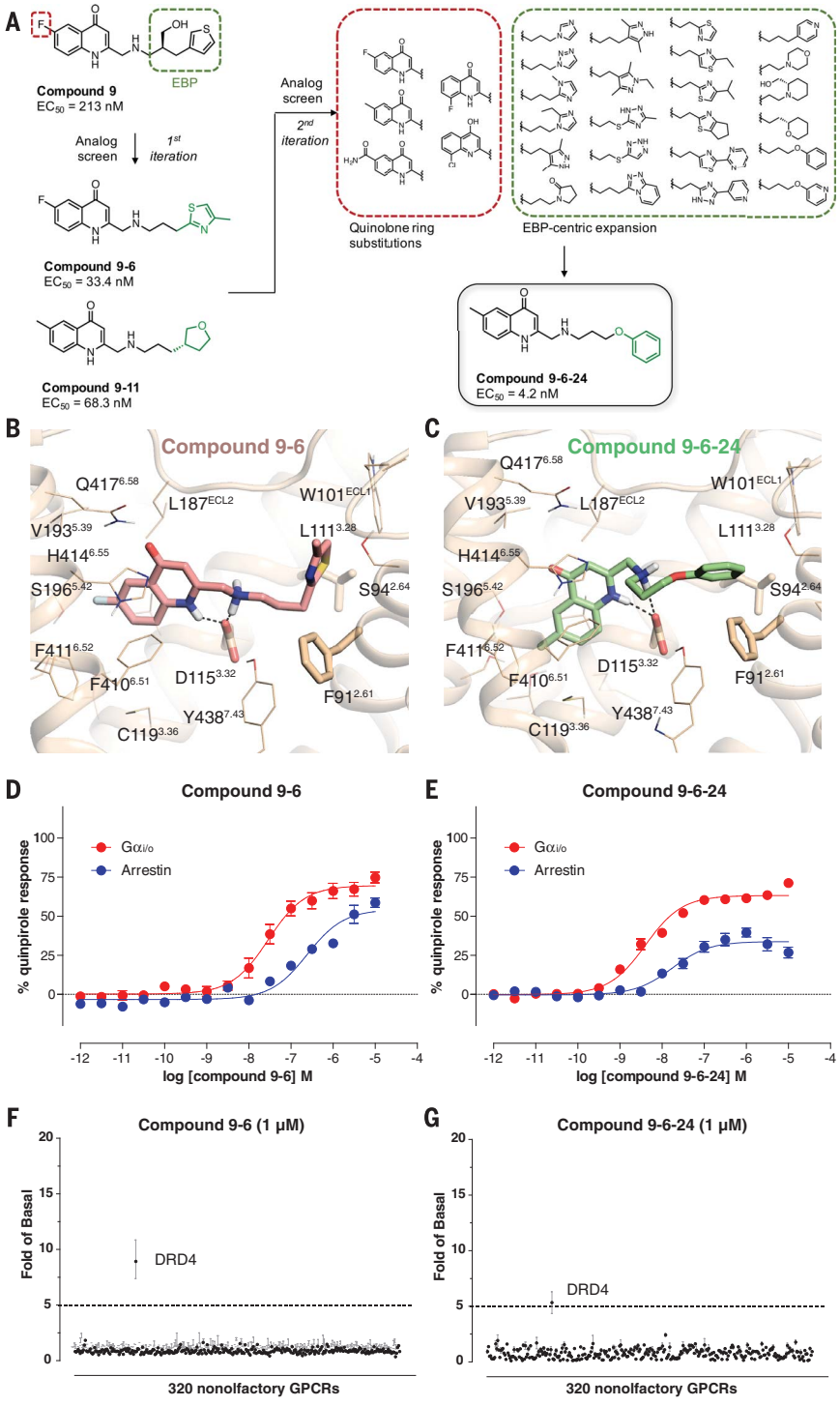

Fig. 4. Structure-guided compound optimization toward potent and selective DRD4 agonists. (**A**) Overview of structure-guided "analog-by-catalog" optimization toward compound **9-6-24**. EC_{50}, median effective concentration. (**B** and **C**) Docking poses of compounds **9-6** (B) and **9-6-24** (C). Both optimized analogs have a simplified right-hand linker while maintaining key interactions and occupying the EBP. DRD4 is shown in tan, and compounds are shown as capped sticks with carbons colored pink (compound **9-6**) and green (compound **9-6-24**). Ballesteros-Weinstein numbering is shown in superscript. (**D** and **E**) Normalized concentration-response studies for compounds **9-6** (D) and **9-6-24** (E) in human-cloned DRD4-mediated activation of $G\alpha_{i/o}$ and arrestin translocation. Error bars, SEM from a minimum of three assays. Details regarding bias factor calculation can be found in the methods. (**F** and **G**) Compounds **9-6** (F) and **9-6-24** (G) were screened against 320 nonolfactory GPCRs for agonism in the arrestin recruitment TANGO assay. Each point shows luminescence normalized to the basal level at a given GPCR. Error bars, SEM.

available to the community to use as probes for DRD4 function, under the names UCSF924 and UCSF924NC, respectively (table S11).

Herein we present a combination of structural, computational, and biochemical studies that illuminates the structure and function of DRD4 at atomic resolution. We further show that leveraging high-resolution structural data in ligand discovery campaigns guided by pharmacological assays can rapidly uncover previously unrecognized, potent, and highly selective probes with desired functional properties.

REFERENCES AND NOTES

1. C. Missale, S. R. Nash, S. W. Robinson, M. Jaber, M. G. Caron, *Physiol. Rev.* **78**, 189–225 (1998).
2. J. M. Beaulieu, S. Espinoza, R. R. Gainetdinov, *Br. J. Pharmacol.* **172**, 1–23 (2015).
3. E. Y. Chien *et al.*, *Science* **330**, 1091–1095 (2010).
4. R. Chu *et al.*, *J. Mol. Biol.* **323**, 253–262 (2002).
5. S. G. Rasmussen *et al.*, *Nature* **477**, 549–555 (2011).
6. W. Liu *et al.*, *Science* **337**, 232–236 (2012).
7. G. Fenalti *et al.*, *Nature* **506**, 191–196 (2014).
8. J. L. Miller-Gallacher *et al.*, *PLOS ONE* **9**, e92727 (2014).
9. C. Zhang *et al.*, *Nature* **492**, 387–392 (2012).
10. V. Katritch *et al.*, *Trends Biochem. Sci.* **39**, 233–244 (2014).
11. H. Gutiérrez-de-Terán *et al.*, *Structure* **21**, 2175–2185 (2013).
12. O. N. Vickery, J. P. Machtens, G. Tamburrino, D. Seeliger, U. Zachariae, *Structure* **24**, 997–1007 (2016).
13. K. A. Neve, *Mol. Pharmacol.* **39**, 570–578 (1991).
14. M. Michino, R. B. Free, T. B. Doyle, D. R. Sibley, L. Shi, *Chem. Commun. (Camb.)* **51**, 8618–8621 (2015).
15. M. M. Simpson *et al.*, *Mol. Pharmacol.* **56**, 1116–1126 (1999).
16. J. A. Schetz, P. S. Benjamin, D. R. Sibley, *Mol. Pharmacol.* **57**, 144–152 (2000).
17. A. H. Newman *et al.*, *J. Med. Chem.* **55**, 6689–6699 (2012).
18. M. Michino *et al.*, *Mol. Pharmacol.* **84**, 854–864 (2013).
19. T. I. Oprea, A. M. Davis, S. J. Teague, P. D. Leeson, *J. Chem. Inf. Comput. Sci.* **41**, 1308–1315 (2001).
20. T. Sterling, J. J. Irwin, *J. Chem. Inf. Model.* **55**, 2324–2337 (2015).
21. A. Manglik *et al.*, *Nature* **537**, 185–190 (2016).
22. K. Lansu *et al.*, *Nat. Chem. Biol.* **13**, 529–536 (2017).
23. A. P. Bento *et al.*, *Nucleic Acids Res.* **42**, D1083–D1090 (2014).
24. A. Negri *et al.*, *J. Chem. Inf. Model.* **53**, 521–526 (2013).
25. D. Wacker *et al.*, *Cell* **168**, 377–389.e12 (2017).

ACKNOWLEDGMENTS

This work was supported by the NIH (grants R01MH112205, U19MH82441, and HHSN-271-2013-00017-C), the Michael Hooker Chair for Protein Therapeutics and Translational Proteomics (to B.L.R.), and the National Institute of General Medical Sciences (NIGMS; grant R35GM122481 to B.K.S.). We thank J. Sondek and S. Endo-Streeter for independent structure quality-control analysis; M. J. Miley and the University of North Carolina macromolecular crystallization core facility supported by the NIH (grant P30CA016086); J. W. Murphy for running FRAP (fluorescence recovery after photobleaching) precrystallization assays; S. Sato for sharing the original DRD4 construct; B. E. Krumm for advice on data processing; and J. Smith, R. Fischetti, and the staff of GM/CA @ APS, supported by the National Cancer Institute (ACB-12002) and NIGMS (AGM-12006). This research used resources of the Advanced Photon Source, a U.S. Department of Energy (DOE) Office of Science User Facility operated for the DOE Office of Science by Argonne National Laboratory under contract no. DE-AC02-06CH11357. Coordinates and structure factors have been deposited in the Protein Data Bank under accession numbers 5WIU (sodium-free) and 5WIV (sodium-bound). UCSF924 and its deactivated negative control UCSF924NC are available as a probe pair from Sigma Millipore (SML2022 and SML2023 for the active and deactivated agonists, respectively).

SUPPLEMENTARY MATERIALS

www.sciencemag.org/content/358/6361/381/suppl/DC1
Materials and Methods
Figs. S1 to S16
Tables S1 to S13
References (*26*–*64*)
Data S1

28 April 2017; accepted 7 September 2017
10.1126/science.aan5468

Science

D4 dopamine receptor high-resolution structures enable the discovery of selective agonists

Sheng WangDaniel WackerAnat LevitTao CheRobin M. BetzJohn D. McCorvyA. J. VenkatakrishnanXi-Ping HuangRon O. DrorBrian K. ShoichetBryan L. Roth

Science, 358 (6361), • DOI: 10.1126/science.aan5468

A strategy for drug discovery

Dopamine receptors are G protein-coupled receptors implicated in many neurological disorders. Different families of dopamine receptors are involved in different signaling pathways, so specificity is a key goal of therapeutics. Wang *et al.* present high-resolution crystal structures of the DRD4 dopamine receptor bound to the antipsychotic drug nemonapride. The high resolution of the structures facilitated ligand docking, and a DRD4-selective agonist was identified by computational screening of a large library, experimental testing of compounds with the best docking scores, and iterative cycles of docking and testing analogs of those compounds. The identified agonist had a high affinity for DRD4 and no measurable affinity for DRD2 or DRD3.

Science, this issue p. 381

Science (ISSN 1095-9203) is published by the American Association for the Advancement of Science. 1200 New York Avenue NW, Washington, DC 20005. The title *Science* is a registered trademark of AAAS.